IOPscience iopscience.iop.org

Home Search Collections Journals About Contact us My IOPscience

Integral evaluation in the mathematical and numerical modelling of high-electron-mobility transistors

This article has been downloaded from IOPscience. Please scroll down to see the full text article.

2001 J. Phys.: Condens. Matter 13 515

(http://iopscience.iop.org/0953-8984/13/3/311)

View the table of contents for this issue, or go to the journal homepage for more

Download details:
IP Address: 171.66.16.226
The article was downloaded on 16/05/2010 at 08:20

Please note that terms and conditions apply.

INSTITUTE OF PHYSICS PUBLISHING JOURNAL OF PHYSICS: CONDENSED MATTER

J. Phys.: Condens. Matter **13** (2001) 515–524 www.iop.org/Journals/cm PII: S0953-8984(01)16921-3

Integral evaluation in the mathematical and numerical modelling of high-electron-mobility transistors

Eric A B Cole

Department of Applied Mathematics, University of Leeds, Leeds LS2 9JT, UK

Received 7 September 2000, in final form 6 November 2000

Abstract

The main processes involved in the mathematical and numerical modelling of high-electron-mobility transistors are presented. The governing equations must be solved rapidly and accurately for the simulation to be of use in CAD (computer-aided design) packages. New analytic approximations are derived for certain integrals which arise in the simulation, enabling these integrals to be calculated rapidly. Results produced in this way are compared with those produced using earlier less accurate approximations.

1. Introduction

Mathematical and numerical modelling plays a vital role in the design and manufacture of new microwave devices. It is a modeller's goal to produce fast and accurate solutions of the modelling equations for use in CAD packages. In this paper we will concentrate on the problem of evaluating certain integrals encountered in the modelling of the high-electron-mobility transistor (HEMT), and present new ways of rapidly and accurately evaluating these integrals.

The HEMT is a multilayer device with three contacts—the ohmic source, Schottky gate and ohmic drain. Figure 1 shows a device cross-section in the x–y plane, and illustrates a typical eight-layer device consisting of layers of gallium arsenide (GaAs), aluminium gallium arsenide (AlGaAs) and indium gallium arsenide (InGaAs). The length of the gate is usually in the range of 0.1 μm to 1.0 μm while the thickness in the y-direction (across the layer structure) is usually of the range of 0.1 μm to 0.5 μm. The depth in the z-direction is normally in the range 10 μm through to 1 mm, and this comparatively large size very often enables a two-dimensional solution to suffice. Higher operating frequencies are produced by shorter-gate-length devices. Voltages V_s and V_d on the source and drain cause a current to flow through the device, and this current is modulated by varying the voltage V_g on the gate; this causes greater or lesser depletion of the charge carriers around the gate leading to a narrowing or widening of the conduction channel through which the charge carriers pass.

In the HEMT, the electron current dominates and it is normal to consider only electron transport through the device (the unipolar model). Fast operation of the HEMT device is achieved when excess carrier electrons are generated in the AlGaAs and fall into the potential wells formed at the layer interfaces. Here they suffer fewer collisions with lattice sites and

0953-8984/01/030515+10$30.00 © 2001 IOP Publishing Ltd Printed in the UK

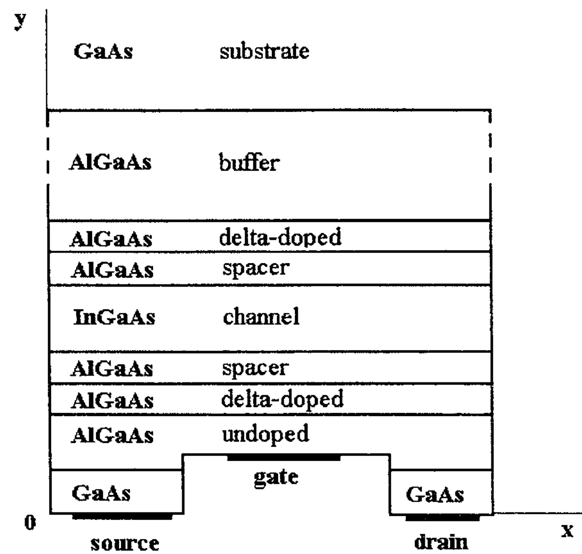

Figure 1. A schematic cross-section of a four-layer device.

move rapidly through the device. These potential wells cause the energies allowed to the electrons to be quantized, and the quantum solution greatly adds to the cost of producing numerical results.

The modelling of such a system can be done in several ways. In the *equivalent-circuit* method [1] used in many CAD packages the characteristics of the device are modelled by constructing an equivalent electrical circuit mimicking the electrical responses at the device terminals. However, these characteristics depend crucially on the geometry of the device and on the underlying solid-state processes, and the equivalent circuit method is not capable of adequately taking these subtleties into account. In the *Monte Carlo* simulation technique [2, 3] the trajectories of all the electrons in the device are followed when the electronic band structure and scattering rates are given. The electron density in the device can be typically of the order of 10^{23} m^{-3}, and although this approach allows a powerful insight into device operation it is extremely expensive in computing terms. The method used in this paper will be that of *semiclassical modelling* in which the Poisson equation together with the first three moments of the Boltzmann transport equation provide partial differential equations [4–9]. These equations contain coefficients such as mobility and relaxation times whose dependence on particle energy are assumed known from Monte Carlo simulations performed previously (often in a semiclassical environment). The modelling of the HEMT requires the addition of the Schrödinger equation from quantum mechanics for a self-consistent solution to account for quantization of electrons in the exceptionally thin layer structure [10]. As detailed below, the integrals whose evaluation is the theme of this paper occur in the link between the quantized solutions and the expression for the electron density.

2. The semiclassical modelling equations

It is normal to take a two-dimensional model in which the length in the z-direction is large enough for changes in that direction to be neglected. The physical quantities which provide a description of the processes are the electrostatic potential $\psi(x, y)$, the electron density

$n(x, y)$ and the electron temperature $T(x, y)$. All three quantities depend on position and time, while the lattice temperature T_0 is assumed for simplicity to be a constant value in this work. The equations and associated boundary conditions used in the semiclassical method are the Poisson equation, electron continuity equation, the energy transport equation and the Schrödinger equation. The second and third of these will not be detailed here, but have been described fully elsewhere [7, 10]. The Poisson equation is

$$\nabla \cdot (\epsilon_0 \epsilon_r \nabla \psi) = -q(N_D - n) \tag{2.1}$$

where $q = 1.6 \times 10^{-19}$ C is the magnitude of the electron charge, ϵ_0 and ϵ_r are the permittivities of the vacuum and the material, respectively, and N_D is the layer-dependent doping density of the material which is fixed in the manufacturing process. The electric field is $\boldsymbol{E} = -\nabla \psi$.

Since potential wells are formed near the AlGaAs–GaAs–InGaAs interfaces, we must also solve the Schrödinger equation in a self-consistent manner along with the equations of current continuity, energy transport and Poisson. The offset band structure between the different layers is shown in figure 2, and the step E_h depends on the mole fraction u of Al or In in the AlGaAs or InGaAs. The Schrödinger equation which must be solved is

$$-\frac{\hbar^2}{2} \nabla \cdot \left(\frac{1}{m^*} \nabla \xi_i \right) + (V_{xc} + E_h - q\psi)\xi_i = q\lambda_i \xi_i \tag{2.2}$$

where $\hbar$ is the reduced Planck constant, and ξ_i and λ_i $(i = 0, 1, \ldots)$ are the energy eigenfunctions and eigenvalues respectively. The effective mass m^* is a function of position, and the form of the kinetic energy operator in equation (2.2) is taken to reflect the fact that it is a Hermitian operator. The quantity V_{xc} is the exchange correlation energy which is a function of position and electron density n [10]. In terms of the fraction u of Al in the AlGaAs, we take [13] the effective electron mass m^* as $m^* = (0.067 + 0.083u)m_e$ where m_e is the constant electron mass, $E_h = 0.65(1.155u - 0.37u^2)$ and the permittivity of the material as $\epsilon_r = 13.18 - 3.12u$. Similar results hold for InGaAs.

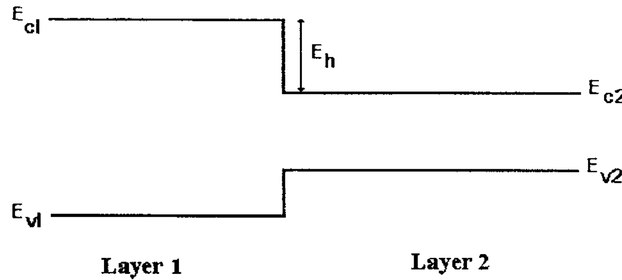

Figure 2. The band offset structure of different layers.

The process of obtaining the full two-dimensional solution of the Schrödinger equation for the eigenfunctions and eigenvalues is very time consuming. It is therefore usual to solve the equation in one-dimensional slices perpendicular to the layer structure, and to impose the boundary conditions $\xi_i(y = 0) = \xi_i(y = Y) = 0$ $(i = 0, 1, \ldots)$ on the eigenfunctions. This is also justifiable since there is little or no quantization in the x-direction. In order to solve this equation the electrostatic potential ψ must be calculated from the Poisson equation (2.1) whose right-hand side requires the electron density n to be calculated. This is given as $n = n_2 + n_3$ where n_2 is the contribution from the sub-bands given by the Schrödinger equation and n_3 is the contribution from the bulk electron density. Specifically, *outside* the potential well we

have $n_2 = 0$ and

$$n_3 = N_{c3} F_{1/2}\left(\frac{q}{k_B T}(E_F - E_c)\right) \tag{2.3}$$

where

$$N_{c3} \equiv 2\left(\frac{m^* k_B T}{2\pi\hbar^2}\right)^{3/2}$$

and E_F is the Fermi level and E_C the conduction band minimum. The Fermi integral F_r is defined in equation (3.2). *Inside* the potential well we calculate the discrete energy levels up to some position-dependent well-top energy E_{top} and take

$$n_2 = N_{c2} \sum_{\lambda_j \leqslant E_{top}} |\xi_j(y)|^2 \ln\left(1 + \exp\left(\frac{q}{kT}(E_F - \lambda_j)\right)\right) \tag{2.4}$$

where

$$N_{c2} \equiv \frac{m^* kT}{\pi\hbar^2}$$

and

$$n_3 = \frac{1}{2}\pi\left(\frac{8m^*}{4\pi^2\hbar^2}\right)^{3/2} q^{3/2} \int_{E_{top}}^{\infty} \frac{(E - E_c)^{1/2}}{1 + \exp([q/(k_B T)](E - E_F))}\, \mathrm{d}E. \tag{2.5}$$

Here the extreme non-linearity of the problem becomes apparent; the solution ψ of the Poisson equation requires an expression for n on the right-hand side, n itself is calculated from the eigensolutions of the Schrödinger equation and these are solved using a potential which depends on ψ. One problem at this stage is to define what is meant by the top of the potential well specified by the energy E_{top}. One approach [14] has been to calculate the energy eigenvalues until the difference between consecutive values falls below the thermal energy $k_B T/q$. However, this may not be adequate for some complex well structures in which the energy eigenvalues lie in close pairs. This fact is illustrated in table 2 (see later) for the results of the first ten eigenvalues of the simulation. The numerical solution of the Schrödinger equation also adds considerably to the computational effort of the problem, and the solution scheme should aim to compute only a relatively small number of eigensolutions. It is therefore desirable to take a value of E_{top} which is as small as possible, since a larger value would require the calculation of more eigensolutions for use in the expression (2.4) for n_2. When the value of E_{top} (or rather, the number of eigensolutions to be used) has been chosen, the conduction band minimum E_c is then taken as $\max(E_h - \psi, E_{top})$. The Fermi energy E_F has been introduced in equations (2.3) and (2.4), and in order to avoid having to calculate E_F by inverting these equations we use ψ, E_F and T as the dependent variables. Appropriate boundary conditions can be calculated for E_F in terms of those already used for ψ, n and T.

The coding of the Fermi integral in equation (2.3) is straightforward using good analytic approximations [15], but the coding of the integral in equation (2.5) presents difficulty. It is desirable to have an analytic expression for this integral so that derivatives for use in the elements of the Jacobian matrix which is used in Newton iteration may be evaluated easily. In the next section we develop analytic approximations for this integral and similar ones which allow for their rapid calculation. These integrals will be of the general form

$$I_r(a, b) \equiv \frac{1}{\Gamma(r+1)} \int_0^{\infty} \frac{(x+b)^r}{1 + \mathrm{e}^{x-a}}\, \mathrm{d}x \tag{2.6}$$

where

$$\Gamma(r+1) \equiv \int_0^{\infty} x^r \mathrm{e}^{-x}\, \mathrm{d}x.$$

In terms of these integrals, equation (2.5) can be written as

$$n_3 = N_{c3} I_{1/2}\left(\frac{q}{k_B T}(E_F - E_{top}), \frac{q}{k_B T}(E_{top} - E_c)\right) \tag{2.7}$$

while the corresponding expressions for the energy density in the full non-degenerate case can be shown *outside* the quantum wells to be

$$W_2 = 0 \qquad W_3 = \frac{3}{2} N_{c3} k_B T F_{3/2}\left(\frac{q}{k_B T}(E_F - E_c)\right) \tag{2.8}$$

and *inside* the wells to be

$$W_2 = N_{c2} k_B T \sum_{\lambda_j \leqslant E_{top}} |\xi_j(y)|^2 I_1\left(\frac{q}{k_B T}(E_F - \lambda_j), \frac{q}{k_B T}(\lambda_j - E_c)\right) \tag{2.9}$$

$$W_3 = \frac{3}{2} N_{c3} k_B T I_{3/2}\left(\frac{q}{k_B T}(E_F - E_{top}), \frac{q}{k_B T}(E_{top} - E_c)\right). \tag{2.10}$$

Thus we see that analytic approximations are needed at least for the integrals $I_{1/2}$, I_1 and $I_{3/2}$. A crude approximation to these integrals [14] in which the second arguments of the I_r-integrals are taken as zero (thereby producing simple Fermi integrals) produces errors, and these errors are quantified in the results which follow.

3. The integrals and their approximations

On making the substitution $x \to x - b$, the integral defined in equation (2.6) can be written as

$$I_r(a, b) \equiv \frac{1}{\Gamma(r+1)} \int_b^\infty \frac{x^r}{1 + \mathrm{e}^{x-(a+b)}}\, \mathrm{d}x. \tag{3.1}$$

The standard Fermi integral has the form

$$F_r(a) \equiv \frac{1}{\Gamma(r+1)} \int_0^\infty \frac{x^r}{1 + \mathrm{e}^{x-a}}\, \mathrm{d}x \tag{3.2}$$

and has the properties

$$F_r'(a) = F_{r-1}(a) \qquad F_r(a) \to \mathrm{e}^a \qquad \text{for } a \ll 0.$$

This last condition is the condition for non-degeneracy, and the replacement of Fermi integrals with exponential functions which are independent of r makes the non-degenerate approximation much easier to use.

The integrals $I_r(a, b)$ have the properties

$$I_r(a, 0) = F_r(a)$$

$$I_0(a, b) = F_0(a) = \ln(1 + \mathrm{e}^a)$$

$$I_1(a, b) = F_1(a) + b \ln(1 + \mathrm{e}^a)$$

$$I_n(a, b) = F_n(a) + b \sum_{r=1}^{n} \frac{1}{r!} b^{r-1} F_{n-r}(a) \qquad n \text{ integer} \geqslant 1 \tag{3.3}$$

$$\frac{\partial}{\partial b} I_r(a, b) = I_{r-1}(a, b) \tag{3.4}$$

$$\frac{\partial}{\partial a} I_r(a, b) = \frac{1}{\Gamma(r+1)} \frac{b^r}{1 + \mathrm{e}^{-a}} + I_{r-1}(a, b). \tag{3.5}$$

Clearly there is no problem in obtaining expressions for the $I_r(a, b)$ when r is an integer, because equation (3.3) shows that it may be written in terms of the Fermi integrals $F_r(a)$

which are easily calculated using the approximations of Bednarczyk and Bednarczyk [15]. However, an approximation is needed for the $\frac{1}{2}$-integral values of r.

In order to approximate these integrals, define the function $c_r(a, b)$ such that

$$I_r(a, b) = F_r(a) + c_r(a, b) \ln(1 + \mathrm{e}^a). \tag{3.6}$$

Since the $F_r(a)$ are easily calculated, the I-integrals are easily evaluated if a simple analytical approximation can be found for the $c_r(a, b)$. In order to do this, look for an approximation in the form

$$c_r(a, b) \approx b^{p_r}(\alpha_r + \beta_r a) \tag{3.7}$$

for some constants p_r, α_r and β_r. The I-integrals are used with arguments a and b given in equations (2.7)–(2.10), and for a typical HEMT these arguments have values typically in the ranges $-8.0 \leqslant a \leqslant 8.0$ and $0 \leqslant b \leqslant 8.0$. We therefore divide the rectangle defined by these ranges into a grid G of points and evaluate the integrals directly at each point. The values of p_r, α_r and β_r are then found which minimize the sum of squares

$$\sum_{(a,b)\epsilon G} \left(\frac{I_r(a, b) - F_r(a)}{\ln(1 + \mathrm{e}^a)} - b^{p_r}(\alpha_r + \beta_r a) \right)^2 .$$

The quantities p_r, α_r and β_r are searched for over suitable ranges which can be lengthened if it is found that the minimum sum of squares falls at the end of an initially chosen range. Table 1 shows the values of p_r, α_r and β_r calculated in this way for several values of r. In calculating these results, grid G was taken with 20×20 points and values were searched for in the ranges

$$0 < p_r < 2r \qquad 0 \leqslant \alpha_r \leqslant 3.0 \qquad -1.0 \leqslant \beta_r \leqslant 1.0.$$

Table 1 also shows the average relative error

$$\left(\sum_{(a,b)\epsilon G} |I_r(a, b) - F_r(a) - b^{p_r}(\alpha_r + \beta_r a) \ln(1 + \mathrm{e}^a)| \right) \Big/ \left(\sum_{(a,b)\epsilon G} |I_r(a, b)| \right)$$

in the I-integral over the chosen range. The form of this relative error is taken to give greater weight to larger values of the integral since these larger values contribute most to the values of n_3 and W_3. It must be stressed that the approximations to the I-integrals obtained in this way do not have the level of global accuracy associated with the approximations to the Fermi integrals of Bednarczyk and Bednarczyk, and are appropriate only to the ranges of a and b given above. For other ranges of a and b, the quantities in the table will need to be re-calculated.

Table 1. Calculated values of p_r, α_r, β_r and the average relative error for various values of r.

r	p_r	α_r	β_r	Error
−1/2	0.2154	−0.3860	0.0294	0.1345
1/2	0.6968	0.5138	−0.0112	0.0193
3/2	1.2937	1.4202	0.0279	0.0348
2	1.5564	1.8126	0.0681	0.0735
5/2	1.8109	2.1184	0.1156	0.1141

With the function $c_r(a, b)$ approximated by expression (3.7) and using the calculated values of the parameters, the integrals $I_r(a, b)$ can rapidly be calculated using equation (3.6). The derivatives needed for use in the Jacobian of the Newton iteration scheme could themselves be found using equations (3.4) and (3.5) although a better convergence of the Newton scheme

will be produced by differentiating equations (3.6) directly:

$$\frac{\partial}{\partial a} I_r(a,b) = F_{r-1}(a) + \beta_r b^{p_r} \ln(1+\mathrm{e}^a) + \frac{c_r(a,b)}{1+\mathrm{e}^{-a}} \tag{3.8}$$

$$\frac{\partial}{\partial b} I_r(a,b) = \frac{p_r}{b} c_r(a,b) \ln(1+\mathrm{e}^a). \tag{3.9}$$

Finally, writing

$$a \equiv \frac{q}{k_B T}(E_F - T_{top}) \qquad b \equiv \frac{q}{k_B T}(T_{top} - E_c)$$

the expressions (2.7) and (2.10) can be written as

$$n_3 = N_{c3} F_{1/2}(a) + n_{3corr}$$

$$W_3 = \frac{3}{2} N_{c3} k_B T F_{3/2}(a) + W_{3corr}$$

where

$$n_{3corr} = N_{c3} c_{1/2}(a,b) \ln(1+\mathrm{e}^a) \tag{3.10}$$

$$W_{3corr} = \frac{3}{2} N_{c3} k_B T c_{3/2}(a,b) \ln(1+\mathrm{e}^a) \tag{3.11}$$

are correction terms to be added to the uncorrected expressions previously used [14].

4. One-dimensional simulation and results

It is not necessary to include current and energy transport across the device in order to illustrate the effectiveness of the integral approximations, since the Poisson and Schrödinger equations alone are closely linked by the expressions for n_2 and n_3. Consequently, this effectiveness may be demonstrated by using a one-dimensional simulation (taken in the y-direction) in which the Poisson and Schrödinger equations are solved self-consistently. The boundary conditions for this one-dimensional simulation will be the same as for a slice through the gate of the two-dimensional model. This model has been considered previously [10] but without the correction terms included. Specifically, we will solve equations (2.1) and (2.2) with the electron densities calculated using equations (2.3), (2.4) and (2.7). For completeness, the energy densities will be calculated from equations (2.8)–(2.10), although only an isothermal model with $T = 300$ K will be considered.

A four-layer AlGaAs–GaAs–AlGaAs–GaAs device will be considered. With the layers numbered from the gate end of the device at $y = 0$, the aluminium fractions u in layers 1–4 are taken as 0.3, 0.0, 0.3 and 0.0 respectively, and the doping density N_D is 1.5×10^{24} m^{-3}, 1.0×10^{20} m^{-3}, 1.5×10^{24} m^{-3} and 1.0×10^{20} m^{-3}. The thicknesses of the layers 1–4 are 30 nm, 20 nm, 20 nm and 100 nm.

The Poisson equation was solved using a multigrid method [10] and the Schrödinger equation was solved at each level to provide updated values for the electron density n. The eigenvalues λ_i were found from the Schrödinger equation using a QL algorithm with implicit shifts and then ordered, with the first few eigenfunctions ξ_i found using back substitution. These eigensolutions were used in the calculation of n_2 using equation (2.4). Table 2 shows the first ten eigenvalues and the differences between each and its preceding value, although only three were used in the calculation of the electron density. Differences which fall below the thermal energy $k_B T/q$ are marked with an asterisk, and indicate that it is not satisfactory to stop calculating eigensolutions when the difference is small in this way. Figure 3 shows a plot of the calculated well structure, with the first three eigenvalues superimposed on the plot

Table 2. The first ten eigenvalues and the difference between each and its preceding value. An asterisk indicates a difference that falls below the thermal energy k_BT/q, which has the value 2.585×10^{-2} eV at $T = 300$ K.

Solution	Eigenvalue (10^{-2} eV)	Difference (10^{-2} eV)
0	−2.689	
1	−1.809	0.880*
2	−0.5214	1.288*
3	2.793	3.314
4	4.284	1.491*
5	5.277	0.993*
6	6.943	1.665*
7	8.143	1.200*
8	9.026	0.883*
9	9.664	0.639*

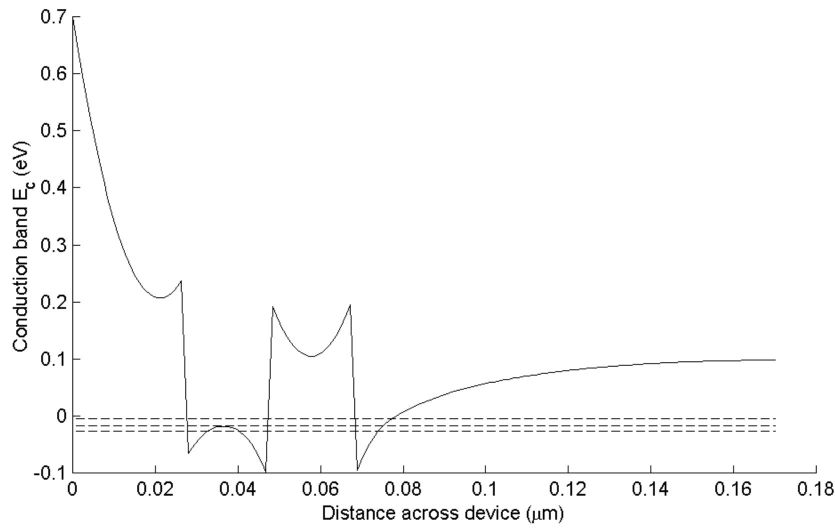

Figure 3. A plot of the conduction band E_c and the first three eigenvalues.

of the conduction band $E_c = E_h - \psi$. Figure 4 shows the plot of the total electron density $n = n_2 + n_3$ together with a plot of the correction term n_{3corr} of equation (3.10). This indicates that a cruder calculation based on replacing the integral $I_{1/2}(a, b)$ by $F_{1/2}(a)$ would produce an electron density reduced by this substantial correction. Figure 5 gives a corresponding comparison for the energy density $W = W_2 + W_3$ together with a plot of the correction term W_{3corr} of equation (3.11). Again, a substantial correction is present.

5. Discussion

The equations modelling the HEMT have been presented. The layer structure of the HEMT is designed to achieve rapid transport of the charge carriers through the device, but this introduces the extra complication of having to solve the Schrödinger equation. The solutions of this equation are used to calculate the electron density by using certain integrals. We have sought to write these integrals in terms of the function $c_r(a, b)$ for which analytic approximations have been derived.

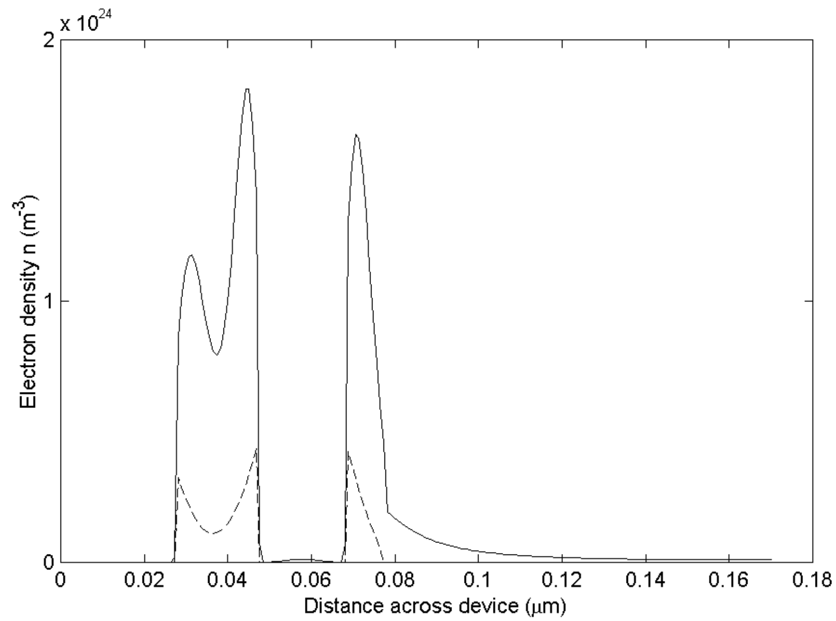

Figure 4. Plots of the total electron density n (solid line) and its correction.

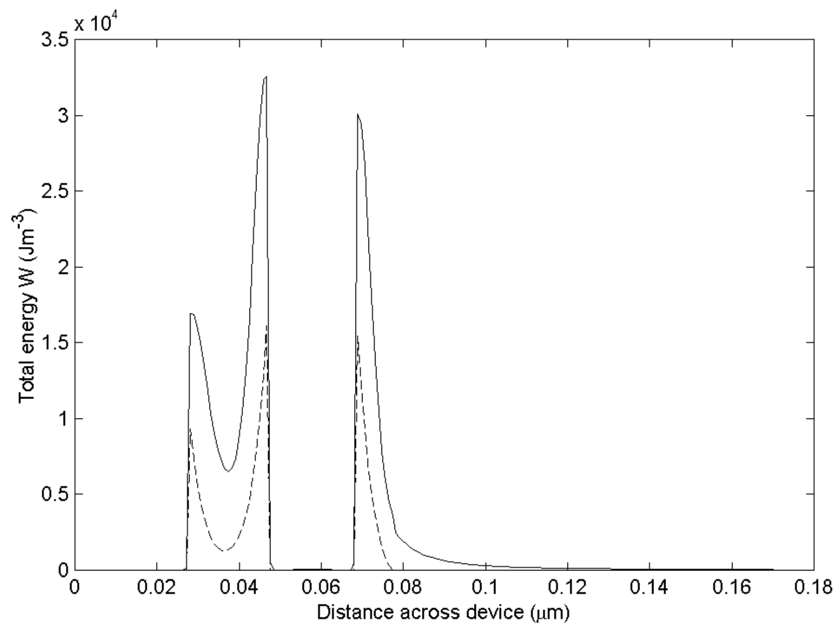

Figure 5. Plots of the total energy density W (solid line) and its correction.

The approximations to the function $c_r(a, b)$ derived here do not have the global status of existing approximations to the Fermi integrals [15]. The values of the parameters p_r, α_r and β_r are derived for ranges of a and b which are applicable to the device considered, although the ranges used here are applicable to the HEMT device in general. If required, it would be

a simple matter to do an automatic re-calculation of the ranges, and hence the parameters, at some intermediate breakpoint in the Newton iteration.

A one-dimensional example of a device with four layers has been used to produce results which indicate the effect of including the correction factor in the calculations. It is sufficient to take a one-dimensional calculation without current and energy transport to show this effect because there is a natural pairing of the Poisson and Schrödinger equations in the model.

Table 2 shows the first ten eigenvalues and the difference between each and its preceding value. An asterisk indicates when a difference falls below the thermal energy $k_B T/q$. This shows that previous methods [14] of stopping the eigensolution calculation when the difference falls below that of the thermal energy are not satisfactory, because the eigenvalues of a multiple-well structure can fall together into very close pairs. Greater accuracy is obviously achieved by using a greater number of eigensolutions but this greatly adds to the computational cost. An indication of the accuracy achieved by taking different numbers of eigensolutions has been given elsewhere [10], although to build an implementation based on this accuracy testing would again greatly increase the computational cost. In order to produce results showing the effect of this correction factor, we have used a fixed arbitrary number (three) of these eigensolutions.

Results shown in figures 4 and 5 indicate that the presence of the correction factor produces appreciable contributions to both the electron density and energy density.

In this paper we have sought to produce analytic approximations to the integrals in order to increase the speed of the numerical implementation consistent with accuracy. As indicated in preliminary investigations [10], this increase should be achieved by being able to take a smaller number of eigensolutions in the calculation of n_2 and W_2. However, we have not sought here to demonstrate how this speed-up will affect the overall efficiency of a complete CAD programme nor how the validity of the analytical approximations applies to different HEMTs; these important considerations will be the subject of further communications.

References

[1] Ieziekiel S 1993 Equivalent circuit modelling *Compound Semiconductor Device Modelling* ed C M Snowden and R E Miles (Berlin: Springer) pp 149–69

[2] Al-Mudares M 1989 Monte Carlo modelling techniques *Semiconductor Device Modelling* ed C M Snowden (Berlin: Springer) pp 180–206

[3] Lugli P 1993 Monte Carlo models and simulations *Compound Semiconductor Device Modelling* ed C M Snowden and R E Miles (Berlin: Springer) pp 210–31

[4] Feng Y-K and Hintz A 1988 Simulation of submicrometer GaAs MESFETS using a full dynamic transport model *IEEE Trans. Electron Devices* **35** 1419–31

[5] Cole E A B 1993 Numerical methods and their application to device modelling *Compound Semiconductor Device Modelling* ed C M Snowden and R E Miles (Berlin: Springer) pp 1–25

[6] Cole E A B and Snowden C M 1995 Numerical algorithms for modelling microwave semiconductor devices *Int. J. Num. Modell.: Electron. Networks, Devices Fields* **8** 13–27

[7] Snowden C M 1989 Classical and semi-classical models *Semiconductor Device Modelling* ed C M Snowden (Berlin: Springer) pp 16–33

[8] Tang T-W 1984 *IEEE Trans. Electron Devices* **31** 1912

[9] McAndrew C C, Singhal K and Heasell E L 1985 *IEEE Electron. Device Lett.* **6** 446

[10] Cole E A B, Snowden C M and Boettcher T 1997 Solution of coupled Poisson–Schrödinger equations using multigrid methods *Int. J. Num. Modell.: Electron. Networks, Devices Fields* **10** 121–36

[11] Selberherr S 1984 *Analysis and Simulation of Semiconductor Devices* (Berlin: Springer)

[12] Singh R 1995 Characterisation and modelling of microwave high electron mobility transistors *PhD Thesis* University of Leeds

[13] Adachi S 1985 *J. Appl. Phys.* **58** R1

[14] Drury R and Snowden C M 1995 *IEEE Trans. Electron Devices* **42** 1026

[15] Bednarczyk D and Bednarczyk J 1978 *Phys. Lett.* A **64** 409